Scientia Iranica B (2021) 28(5), 2628–2638

Sharif University of Technology
Scientia Iranica
Transactions B: Mechanical Engineering
http://scientiairanica.sharif.edu

Observation of stage position in a two-axis nano-positioner using hybrid Kalman filter

S. Bayat[a], H. Nejat Pishkenari[b,*], and H. Salarieh[c]

a. *Department of Industrial and Enterprise Systems Engineering, University of Illinois at Urbana Champaign, Urbana, IL 61801, USA.*
b. *Laboratory of Nano-Robotics, Department of Mechanical Engineering, Sharif University of Technology, Tehran, Iran.*
c. *Department of Mechanical Engineering, Sharif University of Technology, Tehran, Iran.*

Received 16 September 2019; received in revised form 13 November 2020; accepted 30 August 2021

KEYWORDS
Nano positioning stage;
Observer;
Hybrid Kalman filter;
System identification;
Genetic algorithm.

Abstract. This study presents a novel method for observation of stage position in a 2D nano-positioning system based on a hybrid Kalman filter. The proposed method obviates the need to measure the stage position directly using complex and costly capacity sensors. Instead, traditional piezo actuators equipped with strain gauge sensors are utilized to measure the deflection of the magnification system at the position of actuators. Then, a powerful estimation algorithm called Kalman filter was employed to observe stage displacements. The designed hybrid Kalman filter uses dynamical equations of motion in the prediction step. The piezo actuators deflections are measured and exploited to correct the predicted values for the system state variables. In order to simulate realistic conditions, a relatively exact COMSOL model was developed for the nano-positioner. Here, the noise was added to the piezo displacements obtained by simulating this model, and these noisy data were used as measurements in the Kalman filter algorithm. The designed hybrid Kalman filter was examined for three different updating time steps. The results showed that the designed Kalman filter appropriately estimated the stage displacements, and its accuracy was enhanced upon reducing the filter time step.

1. Introduction

With the fast expansion of the application fields of positioning on micro and nano scales such as lithography [1], data storage systems [2], and micro and nano machining [3], design and control of positioning stages have become essential for displacements on nano scales [4–6].

One of the key elements in obtaining proper tracking with little error is to employ feedback signal data used in the controllers [7,8]. Numerous sensors have been proposed to obtain a good feedback signal. Two major characteristics of these sensors are accuracy and displacement range [9–12]. To obtain high absolute accuracy over a large range, laser interferometers can be the best option, hence enjoying a large number of applications [13,14]. One of the other applied sensors is the capacitive sensor [15–18]. These sensors are relatively low-cost and provide a good resolution; however, measuring the capacitance is complex and costly [19,20]. In comparison to these sensors, strain gauge sensors are compact and low-cost [21]. Furthermore, these sensors become highly stable using a full bridge configuration so that they can be used without the intervention of other signals and temperatures [22].

*. *Corresponding author.*
E-mail addresses: bayat2@illinois.edu (S. Bayat); nejat@sharif.edu (H. Nejat Pishkenari); salarieh@sharif.edu (H. Salarieh)

doi: 10.24200/sci.2021.54441.3752

Therefore, achieving long range measurement while keeping the cost at a low level is of high significance due to the increasing availability of long-range nano-positioning mechanisms [23–25].

Although many different sensors have been used in a wide variety of positioning stages in previous studies, in almost all of them, the feedback signal was obtained directly without using any observer. For example, in [6,12,26,27], a number of sensors including optical and capacitive sensors were used directly. Furthermore, sometimes, despite having a piezoelectric actuator equipped with a strain gauge, the feedback signal is obtained using capacitor sensors which in turn increases the cost of the device [28]. The approach used in [4] is to employ Neural Networks and Adaptive neuro fuzzy inference system, thus leading to a reasonable error. To execute that method, some tests should be taken with costly devices to teach the model in advance; however, in the present study, no devices were required, and applying it to the system would lead to a more convenient, inexpensive way of estimating the stage position.

In the scientific world, Kalman filter and its extended format have been used in many applications [29–31]. In this study, a hybrid Kalman filter was designed for a parallel XY nano-positioner in which two strain gauge sensors were used for measuring displacement of piezoelectric actuators. To this end, the nano-positioner system was modeled in COMSOL, and a lumped-linear model was proposed for this system where the parameters of the linearized model were identified in a way that the difference between COMSOL and lumped models was minimized. Afterward, the covariance matrices of the process and observation noises were obtained. Finally, the hybrid Kalman filter was designed, and its sensitivity to three different time steps and five different initial conditions were analyzed. As a result of this process, the observation of stage position of a nano positioner device was done without using any high-tech devices and sensors, which are the basic requirements as seen in the literature [17–19].

This paper is organized as follows: Section 2 introduces the plant, directly measurable state variables, and a brief description of system identification. Section 3 describes the design of a hybrid Kalman filter, whose results are presented in Section 4. Finally, Section 5 concludes the study.

2. Mechanism design

Figure 1 shows the overall schematic view of the nano-positioning system made of Aluminium 7075-T6, and Figure 2 shows its detailed geometry. As observed, piezoelectric actuators apply force on the system, and the displacement of the stage is magnified through a flexural mechanism. There are two piezoelectric

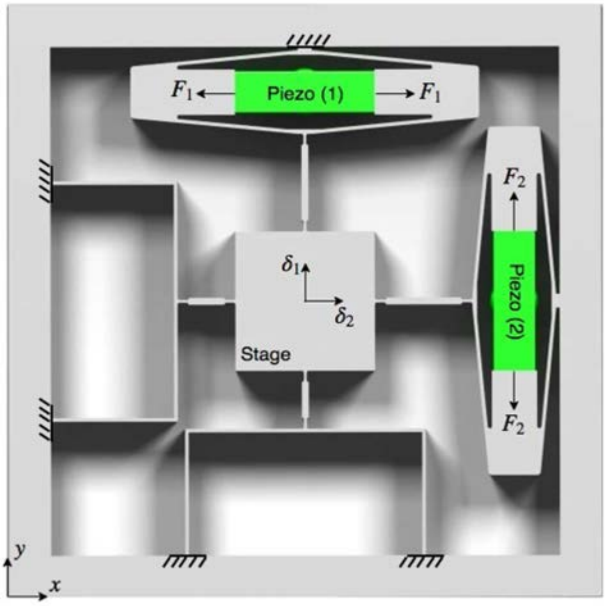

Figure 1. Mechanisms of the nano-positioner: Piezoelectric actuation and corresponding displacements.

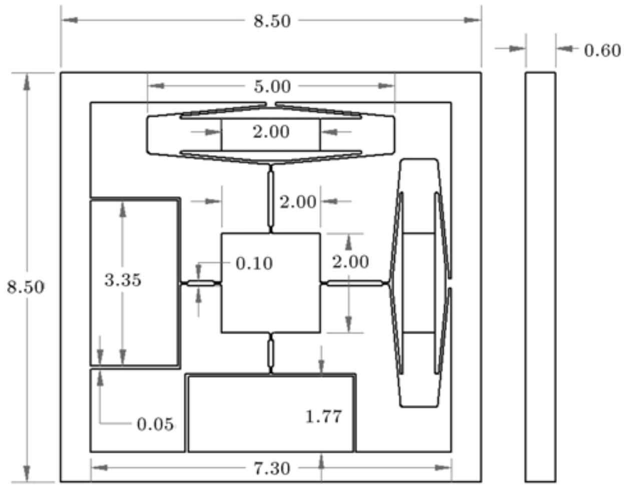

Figure 2. Detailed geometry of the nano-positioner (all dimensions are in cm).

actuators in the mechanism and the length changes of piezoelectric actuators (1) and (2) are in x and y directions, respectively. When actuator (1) is excited, the stage moves along the y direction, while excitation of actuator (2) leads to the stage motion in the x direction.

This mechanism is modeled in COMSOL and as will be discussed in the following sections, simulation data used in the case of hybrid Kalman filter are obtained using COMSOL model. One important point concerning finite element is correct selection of the mesh. In order to obtain appropriate mesh, the natural frequency and displacement of the system were compared for different meshes, and its convergence was the criterion for selecting appropriate mesh.

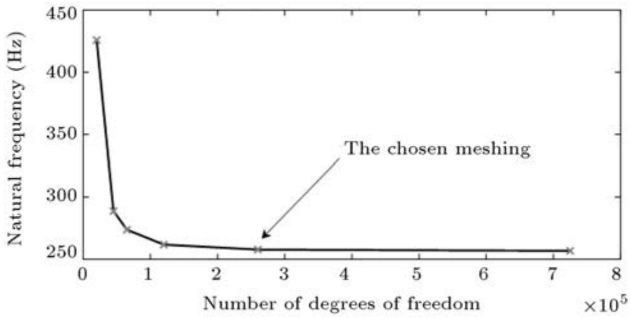

Figure 3. Mesh convergence study.

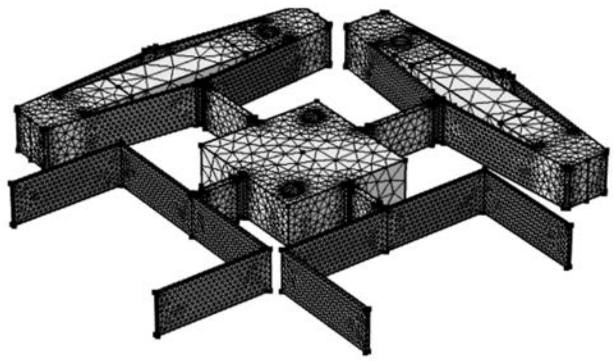

Figure 4. The mesh used in COMSOL model.

Figure 3 shows the convergence of natural frequency for different meshes. In this figure, the vertical axis represents the natural frequency, and the horizontal axis represents the number of degrees of freedom. Note that the number of degrees of freedom depends on the number of elements and their degree of shape function. The final utilized mesh in our study is shown in Figure 4. The COMSOL mesh model includes 46506 Tetrahedral elements, 23742 Triangular Elements, 3659 Edge elements, and 351 Vertex elements.

In order to design a Kalman filter for the considered system, a linearized model of the system is required. As shown in Figure 5, the nano-positioner is modeled with five lumped masses, each having two translational degrees of freedom. As a result, the linearized system has ten degrees of freedom. The linearized dynamics of the system is expressed in Eq. (1):

$$\mathbf{M}\ddot{\mathbf{X}} + \mathbf{C}\dot{\mathbf{X}} + \mathbf{K}\mathbf{X} = \mathbf{F}, \qquad \mathbf{C} = \alpha\mathbf{M} + \beta\mathbf{K}, \tag{1}$$

where $\mathbf{M}$ is the mass matrix, $\mathbf{C}$ the damping matrix, and $\mathbf{K}$ the stiffness matrix. Owing to the symmetry of the system, matrices $\mathbf{M}$, $\mathbf{K}$, and $\mathbf{C}$ are symmetrical with only two parameters which are the equivalent masses of system felt at stage m_1 and actuator locations m_2. These parameters were determined using an optimization procedure and genetic algorithm to narrow down the difference between COMSOL and linearized models. In genetic algorithm, the population size is 50 and the maximum iteration is set as 100.

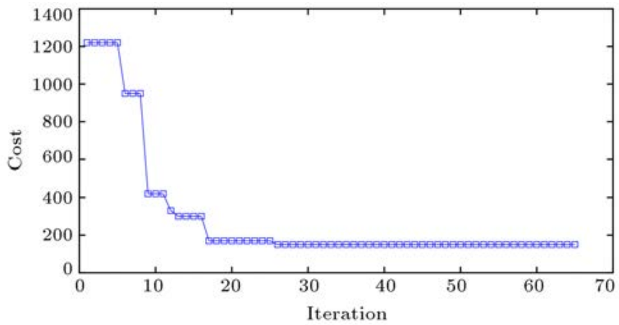

Figure 6. Cost function versus iteration based on genetic algorithm optimization method.

Figure 6 shows the cost function, according to which the cost function is decreasing in the genetic algorithm process, and from the step 30 onwards, it is almost constant and finally, converges at step 65.

After determining the parameters based on the genetic algorithm, we can define the mass, stiffness,

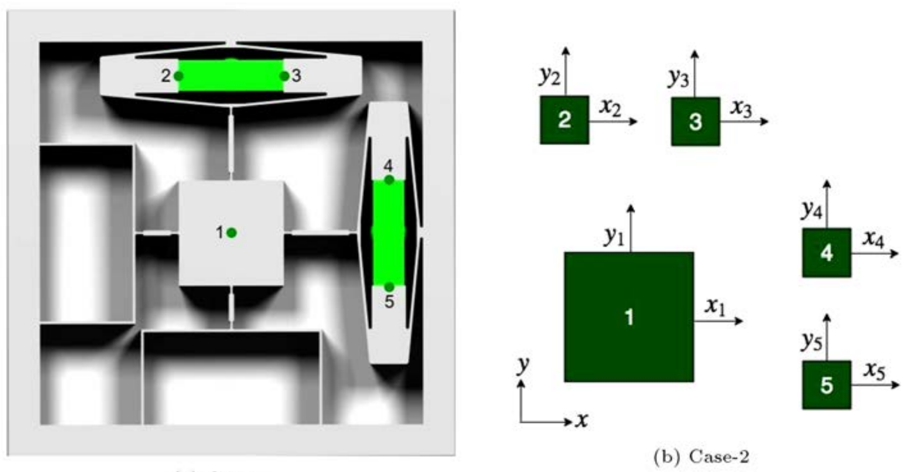

Figure 5. Plant model in COMSOL and the corresponding linearized lumped model.

$$\mathbf{M}=\begin{bmatrix}0.0321I_{2\times 2} & 0_{2\times 8}\\ 0_{8\times 2} & 0.0011I_{8\times 8}\end{bmatrix}, \tag{2}$$

$$\mathbf{K}=\begin{bmatrix}
0.017 & -0.0002 & -0.006 & 0.0008 & 0.0045 & -0.008 & -0.0021 & -0.0972 & -0.0019 & 0.0969\\
-0.0002 & 0.017 & 0.0969 & -0.002 & -0.0974 & -0.002 & -0.0002 & 0.0035 & 0.0002 & -0.007\\
-0.006 & 0.0969 & 1.7916 & 0.0901 & 0.0557 & -1.4811 & 0.0041 & 0.0735 & -0.0042 & -0.0868\\
0.0008 & -0.002 & 0.0901 & 0.0557 & 0.0896 & -0.0515 & -0.0006 & -0.0039 & 0.0005 & 0.0055\\
0.0045 & -0.0974 & -1.4811 & 0.0896 & 1.794 & -0.0908 & -0.0057 & -0.0862 & -0.0057 & 0.1071\\
-0.008 & -0.002 & -0.0889 & -0.0515 & -0.908 & 0.0557 & 0.0006 & 0.004 & -0.0006 & -0.0056\\
-0.0021 & -0.0002 & 0.0041 & -0.0006 & -0.0057 & 0.0006 & 0.0557 & -0.0901 & -0.0515 & -0.0894\\
-0.0972 & 0.0035 & 0.0735 & -0.0039 & -0.0862 & 0.004 & -0.0901 & 1.7916 & 0.0889 & -1.482\\
-0.0019 & 0.0002 & -0.0042 & 0.0005 & 0.0057 & -0.0006 & -0.0515 & 0.0889 & 0.055 & 0.0906\\
0.0969 & -0.007 & -0.0868 & 0.0055 & 0.1071 & -0.0056 & -0.0894 & -1.482 & 0.0906 & 1.7935
\end{bmatrix}, \tag{3}$$

$$\mathbf{C}=0.627\mathbf{M}+0.0001\mathbf{K}. \tag{4}$$

Box I

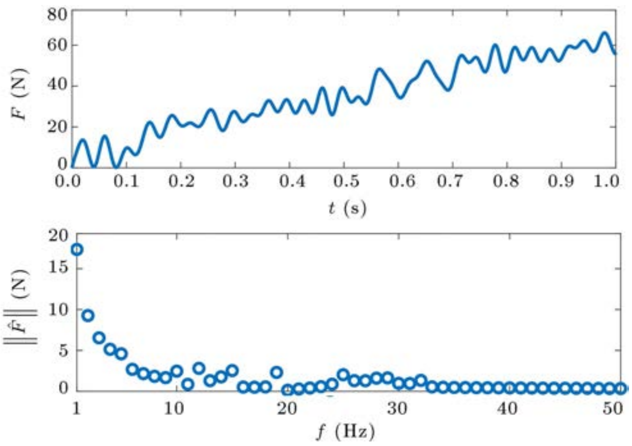

Figure 7. Low frequency signal used for comparison between COMSOL and linear model.

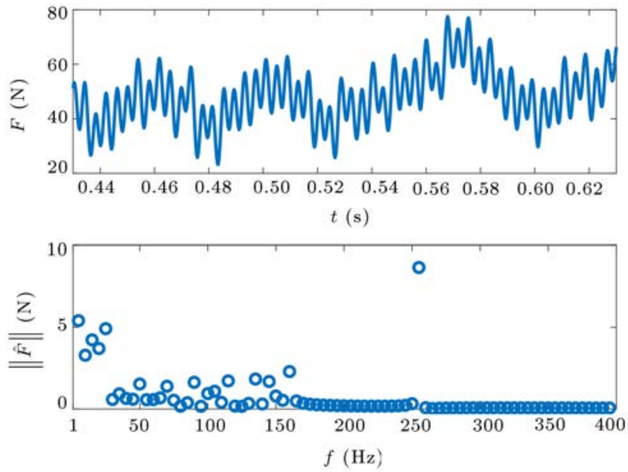

Figure 8. High-frequency signal used for comparison between COMSOL and linear model.

and damping matrices. These are displayed in Eqs. (2)–(4) as shown in Box I. To compare this linear model with COMSOL, two different input signals should be considered. The first one, shown in Figure 7 both in time and frequency domains, is a low frequency signal (up to 33 Hz); and the other one, shown in Figure 8, is a high-frequency signal (up to 260 Hz).

In Figures 9 and 10, the response of the linear model is compared with that of the COMSOL model in terms of low frequency and high frequency input. The low frequency and high frequency inputs for the linear model matching COMSOL model are 99.8% and 99.1%, respectively. Of note, parameters of Eq. (1) are obtained so that the error in stage movement in the y direction between COMSOL and linear model becomes minimum. Therefore, the errors corresponding to the other state variables for the linear model in Eq. (1) and their corresponding values in COMSOL model are not necessarily that small.

After defining each movement and their derivative as state variables, the linearized system is expressed in Eq. (5):

$$\dot{\mathbf{X}}=\mathbf{AX}+\mathbf{Bu}. \tag{5}$$

According to Figure 5, the state variables of the stage movement are x_1 and y_1. However, these variables could not be directly measured because there was no sensor to measure the stage movement. To solve this problem, a strain gauge was mounted on each piezoelectric actuator. These strain gauges measure the displacements of masses 4 and 5 on the y-axis (piezoelectric displacement) and masses 2 and 3 on the x-axis. Then, the stage displacement (x_1, y_1) was estimated using strain gauge data and linearized Kalman filter model.

In addition, it should be noted that the analog-to-digital converter (ad7190) used for reading the strain

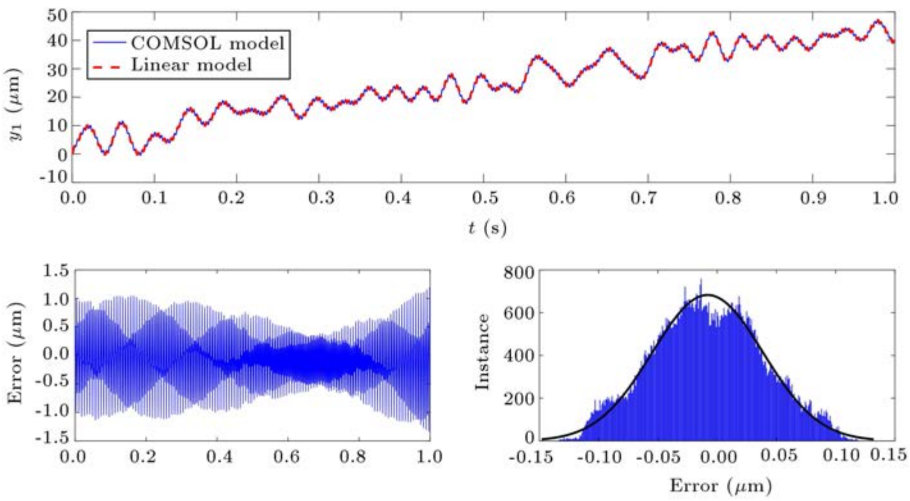

Figure 9. System response to low frequencies after genetic algorithm execution.

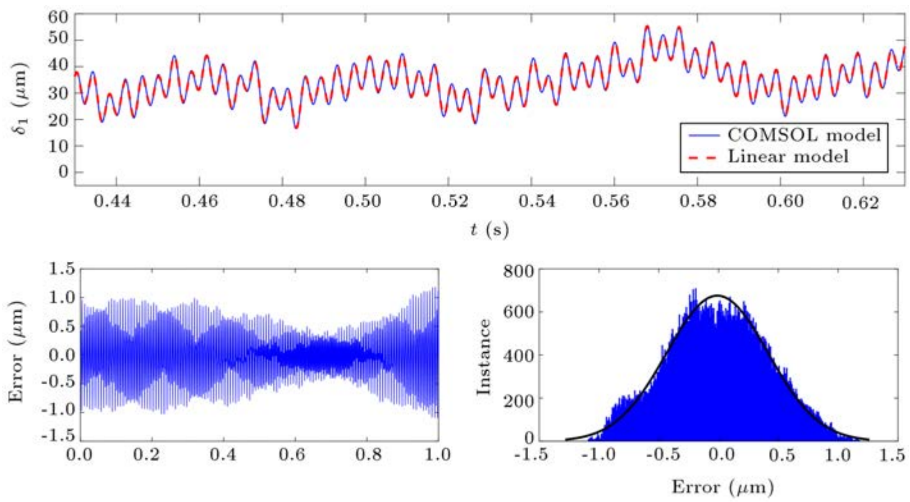

Figure 10. System response to high frequencies after genetic algorithm execution.

gauge signal has a 4.8 kHz maximum output data rate. This frequency should be taken into account while designing Kalman filter because the piezoelectric displacement cannot be measured in time steps faster than 0.21 ms.

3. Hybrid Kalman filter design

The physical system is a continuous-time model whose measurements were done using a digital processor. As a result, a hybrid Kalman filter should be designed to estimate the state variables. The dynamics used in the Kalman filter is shown in Eqs. (6)–(9):

$$\dot{\mathbf{x}}(t) = \mathbf{F}(t)\mathbf{x}(t) + \mathbf{B}(t)\mathbf{u}(t) + \omega(t), \tag{6}$$

$$\mathbf{z}_k = \mathbf{H}_k + \nu_k, \qquad \mathbf{x}_k = \mathbf{x}(t_k), \tag{7}$$

$$\omega \sim \mathbf{N}(0, \mathbf{Q}(t)), \tag{8}$$

$$\nu \sim \mathbf{N}(0, \mathbf{W}_k). \tag{9}$$

In Eqs. (6)–(9), $\mathbf{F}(t)$ is the state transition model, $\mathbf{u}(t)$ the control-input model, and $\omega(t)$ the process noise, which is assumed to be taken from a zero mean multivariable normal distribution $\mathbf{N}$ with covariance $\mathbf{Q}(t)$. In addition, $\mathbf{H}_k$ is the observation model that maps the true state space into the observed space, and ν_k is the observation noise which is assumed to be a zero mean Gaussian white noise with covariance $\mathbf{W}_k$. The Kalman filtering relations for the mentioned model are expressed in Eqs. (10)–(16):

The first phase (prediction):

$$\dot{\hat{\mathbf{x}}}(t) = \mathbf{F}(t)\hat{\mathbf{x}}(t) + \mathbf{B}(t)\mathbf{u}(t),$$

with:

$$\hat{\mathbf{x}}(t_{k-1}) = \hat{\mathbf{x}}_{k-1|k-1} \rightarrow \hat{\mathbf{x}}_{k|k-1} = \hat{\mathbf{x}}(t_k), \tag{10}$$

$$\dot{\mathbf{P}} = \mathbf{F}(t)\mathbf{P}(t)^T + \mathbf{Q}(t),$$

with:

$$\mathbf{P}(t_{k-1}) = \mathbf{P}_{k-1|k-1} \to \mathbf{P}_{k|k-1} = \mathbf{P}(t_k). \quad (11)$$

The second phase (update):

$$\tilde{\mathbf{y}}_k = \mathbf{z}_k - \mathbf{H}_k \hat{\mathbf{x}}_{k|k-1}, \quad (12)$$

$$\mathbf{S}_k = \mathbf{W}_k + \mathbf{H}_k \mathbf{P}_{k|k-1} \mathbf{H}_k^T, \quad (13)$$

$$\mathbf{K}_k = \mathbf{P}_{k|k-1} \mathbf{H}_k^T \mathbf{S}_k^{-1}, \quad (14)$$

$$\hat{\mathbf{x}}_{k|k} = \hat{\mathbf{x}}_{k|k-1} + \mathbf{K}_k \tilde{\mathbf{y}}_k, \quad (15)$$

$$\mathbf{P}_{k|k} = (\mathbf{I} - \mathbf{K}_k \mathbf{H}_k)\, \mathbf{P}_{k|k-1}. \quad (16)$$

In Eqs. (10)–(16), $\hat{\mathbf{x}}_{k|k-1}$ is the estimate for the state variable of step k based on the information up to moment $k-1$, and $\mathbf{P}_{k|k-1}$ is the estimate for the covariance of step k based on the information for the moment $k-1$. According to Eqs. (14) and (15), the gain decreases as the covariance of the noise measurement increases and therefore, the state variables are estimated more based on the dynamics of the system.

To find the model uncertainty covariance matrix, COMSOL model was used as a reference model and the covariance of the process noise is obtained as follows:

COMSOL model:

$$\dot{\mathbf{X}} = \mathbf{F}(\mathbf{X}, \mathbf{u}, t). \quad (17)$$

Linearized model:

$$\dot{\mathbf{X}} = \mathbf{AX} + \mathbf{Bu} + \omega. \quad (18)$$

In accordance with Eqs. (17) and (18), Eq. (19) was proposed to find ω:

$$\omega = \dot{\mathbf{X}}_{\text{COMSOL}} - (\mathbf{AX}_{\text{COMSOL}} + \mathbf{Bu}), \quad (19)$$

where the vector of state variables and its derivatives are obtained using COMSOL model. Since $\mathbf{A}$ and $\mathbf{B}$ are known based on the linear system, the vector ω can be found. Then, matrix $\mathbf{Q}$ is obtained through Eq. (20):

$$\mathbf{Q} = cov(\omega). \quad (20)$$

The dynamic range resolution DNR_{ppm} of resistive strain gauge is considered as 230 in [19]. As a result, the resolution of the strain gauges mounted on the piezo electric actuators, whose full-scale range is nearly 17 μm, is calculated in Eqs. (21) and (22):

$$DNR_{\text{ppm}} = 10^6 \frac{\text{Resplution}}{\text{Full scale range}}, \quad (21)$$

$$\text{Resolution} = DNR_{\text{ppm}} \times \text{Full scale range} \times 10^{-6}$$
$$= 230 \times 17 \times 10^{-3} = 4 \text{ nm}. \quad (22)$$

Here, as a result of the presence of noise in the measurement of the designed device, the standard deviation of the sensor and measurement system as a whole is considered to be 40 nm. Therefore, the covariance of the observation noise, $\mathbf{W}_k$, is obtained through Eq. (24):

$$\nu = 40 \times 10^{-9} \begin{bmatrix} 1 \\ 1 \end{bmatrix}, \quad (23)$$

$$\mathbf{W}_k = (10 \times 10^{-9})^2 \begin{bmatrix} 1 & 0 \\ 0 & 1 \end{bmatrix}. \quad (24)$$

4. Results

In this section, the results of designed hybrid Kalman filter are presented. Since our case study is a nano-positioner, errors are normal on a sub-micrometer scale. According to Figure 5, as stated before, stage movement is a result of piezoelectric actuator excitations. In the COMSOL model, the equivalent forces that piezoelectric actuators exert on masses 2 and 3 as well as 4 and 5 are obtained and applied to the system. The applied force between masses 2 and 3 used for designing Kalman filter is depicted in Figure 11. In addition, the force between masses 4 and 5 is set to be zero.

As shown in Figure 11, the COMSOL model was simulated using the force input, and the state variables data were obtained. Then, a hybrid Kalman filter was designed through the linearized model (Eq. (5)) which used the measurement data obtained by the COMSOL model in the update phase of the Kalman filter.

The hybrid Kalman filter response is presented in Figure 12. As previously mentioned, the AD7190 IC converts the analog signal to digital data, and it can send data up to 4.8 kHz (0.21 milliseconds); therefore, in this simulation, the update rate is measured as 0.3 millisecond, and the difference between the initial conditions of the COMSOL and linearized models is set to 50 μm. In this figure, y_1 is the vertical movement of the stage; "Real" signal is the vertical movement

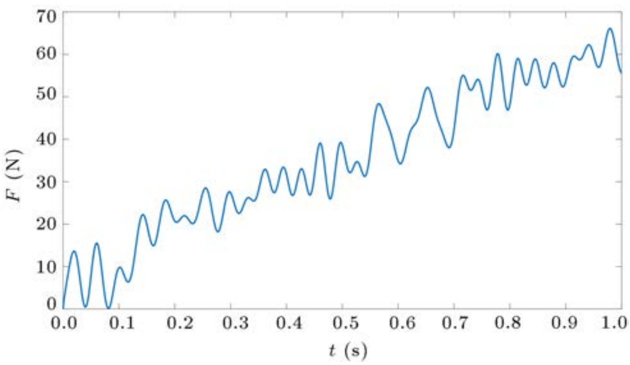

Figure 11. Applied force between masses 4 and 5.

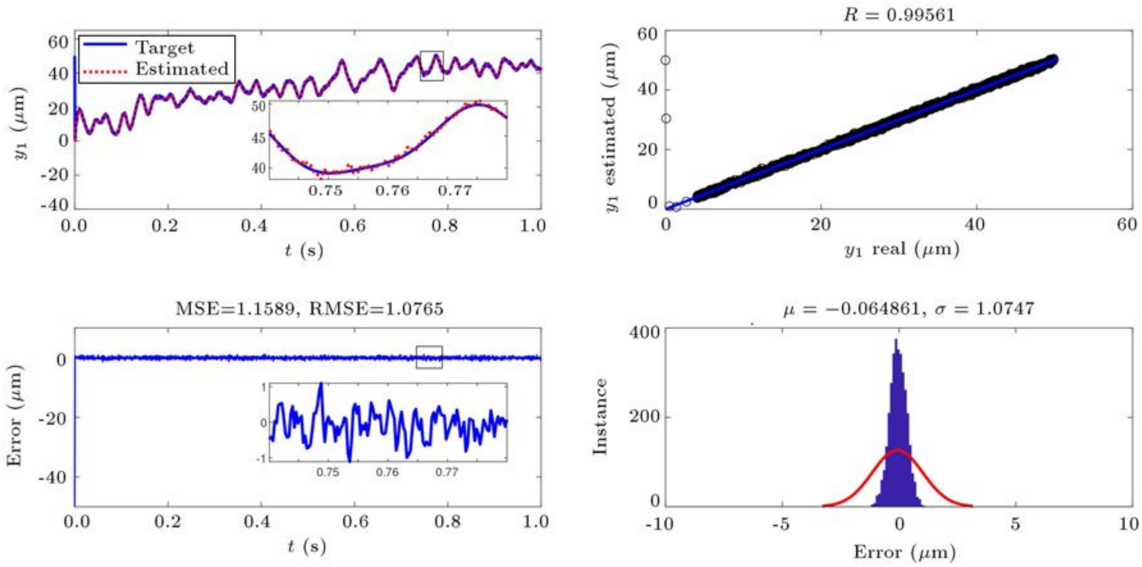

Figure 12. The hybrid Kalman filter response for state variable estimation.

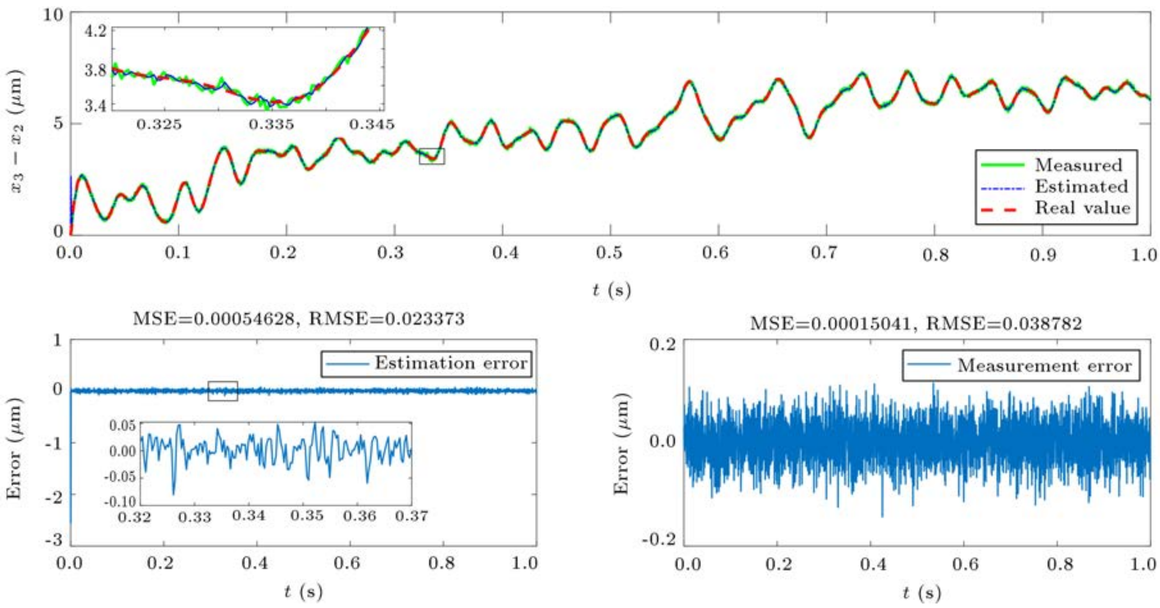

Figure 13. Difference in displacement between masses 2 and 3.

of the stage obtained by the COMSOL model; and "Estimate" signal is the vertical movement of the stage obtained by the Kalman filter.

The characteristics of the Kalman filter were investigated based on correlation (R), standard deviation (σ), mean absolute error (μ), Mean Square Error (MSE), and Root Mean Absolute Error (RMSE). As observed, the designed Kalman filter yielded μ values less than 0.064. Based on the characteristics shown in Figure 12, the designed Kalman filter works appropriately.

In Figure 13, $x_3 - x_2$ is the displacement between masses 2 and 3 (piezoelectric actuator), "Real" data is obtained using the COMSOL model, "Measured" signal is the "Real" data plus some noise that is obtained from Eq. (23), and "Estimated" signal is the Kalman filter estimation. In this figure, while "Estimation Error" is the difference between the "Real" data and "Estimated" signal, "Measurement Error" is the difference between the "Real" and "Measured" signals. As observed, the "Estimated" signal lies somehow in between the "Measured" and "Real"' signals, whose error is less than that of the "Measured" signal. This is due to the application of the Kalman filter that updates the state variables based on the covariance noise of the linearized system and measurements.

Figure 14 shows the simulation of the hybrid Kalman filter under five different initial conditions.

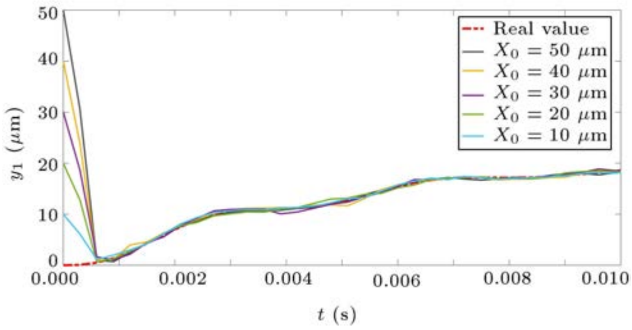

Figure 14. Kalman filter response with different initial conditions.

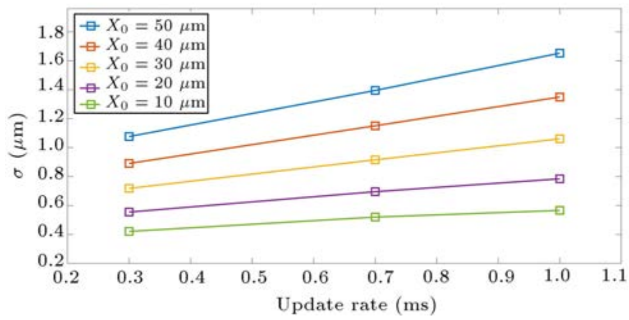

Figure 15. Error of hybrid Kalman filter as a function of update rate for different initial conditions.

As shown in this figure, Kalman model with different initial conditions converges to the real signal obtained from COMSOL model.

The designed hybrid Kalman filter was tested under five different initial conditions and at three different update rates (Table 1). As seen, MSE and all decrease upon increasing the update rate. Furthermore, at higher update rates, R value becomes smaller.

The standard deviation between the COMSOL model and Kalman observer in Table 1, which has fifteen rows, is plotted in Figure 15. As it can be seen, for the initial condition $\mathbf{X}_0 = 50$ μm, the first datum that has a 0.3 ms update rate has lower σ than the second and third data sets that have 0.7 ms and 1 ms update rates, respectively. Furthermore, by comparing each group with a different initial condition, it can be seen that the lower error in the initial condition leads to lower σ.

5. Conclusion

This study performed a hybrid Kalman estimation of a nano-positioning stage based on the term innovation from COMSOL model. It was shown that the error between the linear model obtained by parameter estimation and the COMOSL model was small at both low and high frequencies. Therefore, the linear model yielded a good estimation of the COMOSL model. Furthermore, simulation results demonstrated that the designed Kalman filter could lead to an average error less than 100 nm which is a proper value because, as was mentioned before, running into errors in the

Table 1. Specifications of the hybrid Kalman filter under different initial conditions and at update rates.

Initial condition (μm)	Update rate (ms)	R	MSE (μm^2)	μ (μm)	σ (μm)
$X_0 = 50$	0.3	0.99561	1.1589	–0.064861	1.0747
	0.7	0.99262	1.9458	–0.060387	1.3941
	1	0.98966	2.7309	–0.1014	1.6502
$X_0 = 40$	0.3	0.997	0.79288	–0.065174	0.88819
	0.7	0.99499	1.3242	–0.073503	1.1488
	1	0.99312	1.8212	–0.096632	1.3467
$X_0 = 30$	0.3	0.99805	0.51576	–0.050336	0.71651
	0.7	0.99682	0.83833	–0.05048	0.91453
	1	0.99574	1.1251	–0.058563	1.0596
$X_0 = 20$	0.3	0.99884	0.30757	–0.053031	0.55213
	0.7	0.99819	0.48355	–0.080642	0.69093
	1	0.99768	0.61513	–0.071886	0.78139
$X_0 = 10$	0.3	0.99933	0.17717	–0.036092	0.41942
	0.7	0.99898	0.27025	–0.02	0.51966
	1	0.9988	0.32049	–0.064356	0.56273

sub-micrometer range for a plant used to move with nanometer accuracy was appropriate. Moreover, it should be noted that this error was obtained when the nano-positioner displacement range was up to 60 μm and the measurement noise of the strain gauge sensor was set to 40 nm. At the end, displacements of the nano-positioning stage were obtained using strain gauge sensors and Kalman filter method. In conclusion, our novel method enjoyed the benefits of hybrid Kalman filter and low-cost strain gauges to estimate the stage location in a nano-positioning system. Of note, the existing nano-positioners employ high-cost sensors to directly measure the stage location.

Acknowledgment

The authors would like to gratefully thank Iran National Science Foundation (INSF) for their financial support.

Nomenclature

α	Mass proportional Rayleigh damping coefficient
β	Stiffness proportional Rayleigh damping coefficient
δ_1	Stage movement in y direction
δ_2	Stage movement in x direction
$\dot{\mathbf{X}}$	Velocity of five lumped masses
$\mathbf{X}_{\mathrm{COMSOL}}$	Displacements of five lumped masses obtained from COMSOL
ν_k	Observation noise
ω	Process noise
$\mathbf{A}$	State (or system) matrix
$\mathbf{B}$	Input matrix
$\mathbf{C}$	Damping matrix
$\mathbf{F}$	State transition model
$\mathbf{H}_k$	Observation model
$\mathbf{K}$	Stiffness matrix
MSE	Mean Absolute Error
$\mathbf{M}$	Mass matrix
$\mathbf{N(0,Q(t))}$	Normal distribution with zero mean and $\mathbf{Q}(t)$ covariance
$\mathbf{N(0,W_k)}$	Normal distribution with zero mean and $\mathbf{W}_k$ covariance
$\mathbf{P}$	Estimation of the covariance
$\mathbf{Q}(t)$	Process noise covariance
RMSE	Root Mean Absolute Error
$\mathbf{R}$	Correlation coefficient
$\mathbf{S}_k$	Innovation covariance
$\mathbf{u}$	Input (control) vector
$\mathbf{W}_k$	Observation noise covariance
$\mathbf{X}$	Displacements of five lumped masses
$\mathbf{X}_0$	Initial value
$\mathbf{x}_k$	States at step k
$\mathbf{z}_k$	Measured signal
μ	Mean absolute error
σ	Standard deviation
$\tilde{\mathbf{y}}_k$	Innovation residual
F_1	Equivalent force of piezoelectric (1)
F_2	Equivalent force of piezoelectric (2)
t	Time
x_1	Displacement of lumped mass (1) in x direction
x_2	Displacement of lumped mass (2) in x direction
x_3	Displacement of lumped mass (3) in x direction
x_4	Displacement of lumped mass (4) in x direction
x_5	Displacement of lumped mass (5) in x direction
y_1	Displacement of lumped mass (1) in y direction
y_2	Displacement of lumped mass (2) in y direction
y_3	Displacement of lumped mass (3) in y direction
y_4	Displacement of lumped mass (4) in y direction
y_5	Displacement of lumped mass (5) in y direction
$\dot{\mathbf{X}}_{\mathrm{COMSOL}}$	Velocities of five lumped masses obtained from COMSOL
Piezo (1)	Piezoelectric mounted horizontally (in x direction)
Piezo (2)	Piezoelectric mounted horizontally (in y direction)
Stage	The main plate that moves in x and y direction
x	x direction
y	y direction

References

1. Lee, D., Kim, K., Lee, K., et al. "Robust design of a novel three-axis fine stage for precision positioning in lithography", *Proceedings of the Institution of Mechanical Engineers, Part C: Journal of Mechanical Engineering Science*, **224**(4), pp. 877–888 (2010).
2. Abramovitch, D. and Franklin, G. "A brief history of disk drive control", *IEEE Control Systems Magazine*, **22**(3), pp. 28–42 (2002).

3. Kang, D. and Gweon, D. "Development of flexure based 6-degrees of freedom parallel nano-positioning system with large displacement", *Review of Scientific Instruments*, **83**(3), p. 035003 (2012).

4. Bayat, S., Pishkenari, H.N., and Salarieh, H. "Observer design for a nano-positioning system using neural, fuzzy and anfis networks", *Mechatronics*, **59**, pp. 10–24 (2019).

5. Babahosseini, H., Mahboobi, S.H., Khorsand Vakilzadeh, M., et al. "Optimal sliding mode control for atomic force microscope tip positioning during nano-manipulation process", *Scientia Iranica*, **20**(6), pp. 2285–2296 (2013).

6. Pan, P., Zhu, J., Gu, S., et al. "Development of stick-slip nanopositioning stage capable of moving in vertical direction", *Microsystem Technologies*, **26**(9), pp. 2945–2954 (2020).

7. Korayem, M. and Yousefzadeh, M. "Adaptive control of a cable-actuated parallel manipulator mounted on a platform with differential wheels under payload uncertainty", *Scientia Iranica*, **27**(1), pp. 273–286 (2020).

8. Korayem, M.H., Irani, M., and Rafinekou, S. "Analysis of manipulators using sdre: A closed loop nonlinear optimal control approach", *Scientia Iranica*, **17**(6), pp. 456–467 (2010).

9. George, B., Tan, Z., and Nihtianov, S. "Advances in capacitive, eddy current, and magnetic displacement sensors and corresponding interfaces", *IEEE Transactions on Industrial Electronics*, **64**(12), pp. 9595–9607 (2017).

10. Nguyen, T. and Konishi, S. "Position feedback control for electrostatically controlled linear actuator", *Microsystem Technologies*, **22**(1), pp. 171–179 (2016).

11. Barber, M.E., Steppke, A., Mackenzie, A.P., et al. "Piezoelectric-based uniaxial pressure cell with integrated force and displacement sensors", *Review of Scientific Instruments*, **90**(2), p. 023904 (2019).

12. Mitrovic, A., Leang, K.K., and Clayton, G.M. "Analysis and experimental comparison of range-based control for dual-stage nanopositioners", *Mechatronics*, **69**, p. 102371 (2020).

13. Fleming, A.J. "Nanopositioning system with force feedback for high-performance tracking and vibration control", *IEEE/ASME Transactions on Mechatronics*, **15**(3), pp. 433–447 (2009).

14. Butler, H. "Position control in lithographic equipment: an enabler for current-day chip manufacturing", *IEEE Control Systems*, **31**(5), pp. 28–47 (2011).

15. Golnabi, H. "Measuring small displacements by using a capacitive transducer system", *Scientia Iranica*, **7**(1), pp. 69–74 (2000).

16. Moore, S.I., Fleming, A.J., and Yong, Y.K. "Capacitive instrumentation and sensor fusion for high-bandwidth nanopositioning", *IEEE Sensors Letters*, **3**(8), pp. 1–3 (2019).

17. del Corro, P.G., Imboden, M., Pérez, D.J., et al. "Single ended capacitive selfsensing system for comb drives driven xy nanopositioners", *Sensors and Actuators A: Physical*, **271**, pp. 409–417 (2018).

18. Kang, S., Lee, M.G., and Choi, Y.-M. "Six degrees-of-freedom direct-driven nanopositioning stage using crab-leg flexures", *IEEE/ASME Transactions on Mechatronics*, **25**(2), pp. 513–525 (2020).

19. Fleming, A.J. and Leang, K.K., *Design, Modeling and Control of Nanopositioning Systems*, Springer (2014).

20. Yeh, T.-J., Ruo-Feng, H., and Shin-Wen, L. "An integrated physical model that characterizes creep and hysteresis in piezoelectric actuators", *Simulation Modelling Practice and Theory*, **16**(1), pp. 93–110 (2008).

21. Scaglioni, B., Bascetta, L., Baur, M., et al. "Closed-form control oriented model of highly flexible manipulators", *Applied Mathematical Modelling*, **52**, pp. 174–185 (2017).

22. Schitter, G., Thurner, P.J., and Hansma, P.K. "Design and input-shaping control of a novel scanner for high-speed atomic force microscopy", *Mechatronics*, **18**(5–6), pp. 282–288 (2008).

23. Zhang, Z., Yang, X., and Yan, P. "Large dynamic range tracking of an XY compliant nanomanipulator with cross-axis coupling reduction", *Mechanical Systems and Signal Processing*, **117**, pp. 757–770 (2019).

24. Li, J., Huang, H., and Morita, T. "Stepping piezoelectric actuators with large working stroke for nano-positioning systems: a review", *Sensors and Actuators A: Physical*, **292**, pp. 39–51 (2019).

25. Lee, H.-J., Woo, S., Park, J., et al. "Compact compliant parallel XY nano-positioning stage with high dynamic performance, small crosstalk, and small yaw motion", *Microsystem Technologies*, **24**(6), pp. 2653–2662 (2018).

26. Liu, P., Yan, P., Zhang, Z., et al. "Modeling and control of a novel x-y parallel piezoelectric-actuator driven nanopositioner", *ISA Transactions*, **56**, pp. 145–154 (2015).

27. Shan, Y. and Leang, K.K. "Design and control for high-speed nanopositioning: serialkinematic nanopositioners and repetitive control for nanofabrication", *IEEE Control Systems Magazine*, **33**(6), pp. 86–105 (2013).

28. Qin, Y., Tian, Y., Zhang, D., et al. "Motion control of a 2-dof decoupled compliant mechanism using h synthesis", in *2012 International Conference on Manipulation, Manufacturing and Measurement on the Nanoscale (3M-NANO)*, pp. 222–227, IEEE (2012).

29. Rusdinar, A., Kim, J., Lee, J., et al. "Implementation of real-time positioning system using extended Kalman filter and artificial landmark on ceiling", *Journal of Mechanical Science and Technology*, **26**(3), pp. 949–958 (2012).

30. Dorostgan, M. and Taban, M.R. "Adaptive radar signal detection in autoregressive interference using Kalman-based filters", *Scientia Iranica* (In press). DOI: 10.24200/sci.2019.50136.1534

31. Sheikhbahaei, R., Vossughi, G.R., and Alasty, A. "Optimal tuner selection using Kalman filter for a real-time modular gas turbine model", *Scientia Iranica*, **27**(2), pp. 806–818 (2020).

Biographies

Saeid Bayat graduated with a BSc degree in Mechanical Engineering from the Iran University of Science and Technology in Iran, 2015. He earned his MSc degree in Mechanical Engineering from the Sharif University in 2018 in Tehran, Iran and during this period, he studied the nano-positioning systems. Now, he is a PhD student in University of Illinois at Urbana Champaign and is working on Control Co-Design (CCD) of wind turbines. His fields of research are control co-design, optimization, optimal control, wind turbine control and design, and nano-positioning

Hossein Nejat Pishkenari earned his BSc, MSc, and PhD degrees in Mechanical Engineering from the Sharif University of Technology, Tehran, Iran in 2003, 2005, and 2010, respectively. Then, he joined the Department of Mechanical Engineering at the Sharif University of Technology in 2012. Currently, he is directing the Nano-robotics Laboratory and the corresponding ongoing research projects in the multidisciplinary field of Nanotechnology.

Hassan Salarieh received his BSc in Mechanical Engineering and also Pure Mathematics from Sharif University of Technology, Tehran, Iran in 2002. He graduated from the same university with MSc and PhD degrees in Mechanical Engineering in 2004 and 2008. At present, he is a Professor in the same field at Sharif University of Technology. His fields of research are dynamical systems, control theory, and stochastic systems.